Strain-induced bands of Büngner formation promotes axon growth in 3D tissue-engineered constructs

Carina Hromada[1,2] iD **, Dorota Szwarc-Hofbauer[1,2],
Mai Quyen Nguyen[2,3], Janine Tomasch[1,2]** iD **, Michaela Purtscher[1,2],
David Hercher[1,2,3]* and Andreas Herbert Teuschl-Woller[1,2]***

Abstract
Treatment of peripheral nerve lesions remains a major challenge due to poor functional recovery; hence, ongoing research efforts strive to enhance peripheral nerve repair. In this study, we aimed to establish three-dimensional tissue-engineered bands of Büngner constructs by subjecting Schwann cells (SCs) embedded in fibrin hydrogels to mechanical stimulation. We show for the first time that the application of strain induces (i) longitudinal alignment of SCs resembling bands of Büngner, and (ii) the expression of a pronounced repair SC phenotype as evidenced by upregulation of BDNF, NGF, and p75[NTR]. Furthermore, we show that mechanically aligned SCs provide physical guidance for migrating axons over several millimeters in vitro in a co-culture model with rat dorsal root ganglion explants. Consequently, these constructs hold great therapeutic potential for transplantation into patients and might also provide a physiologically relevant in vitro peripheral nerve model for drug screening or investigation of pathologic or regenerative processes.

Introduction

Peripheral nerve injuries affect up to 5% of all trauma patients and represent a substantial socioeconomic burden due to poor functional recovery, resulting in major healthcare expenses, long sick leaves, and potentially life-long disability as well as unemployability.[1–3]

Notably, peripheral nerves possess an intrinsic capacity to regenerate, which is mainly enabled by the remarkable plasticity of the glial Schwann cells (SCs). Upon injury, SCs undergo a phenotypic change from the mature myelinating state to the regeneration-promoting repair SC state.[4] This process, called adaptive cellular reprograming, involves the downregulation of myelin-associated genes, such as the key transcription factor Krox20, myelin basic protein (MBP), or myelin protein zero (MPZ). Simultaneously, neurotrophic factors are upregulated, including glial cell line-derived neurotrophic factor (GDNF), brain-derived neurotrophic factor (BDNF),

neurotrophin-3, and nerve growth factor (NGF), as well as p75 neurotrophin receptor (p75[NTR]) and N-Cadherin, all of which are able to promote axon regeneration and survival.[5] In addition, SCs secrete cytokines that attract macrophages to aid in myelin debris clearance. Most importantly, SCs proliferate, migrate, and elongate to form bands of Büngner—aligned cellular tracks between the nerve

[1]Department Life Science Engineering, University of Applied Sciences Technikum Wien, Vienna, Austria
[2]The Austrian Cluster for Tissue Regeneration, Vienna, Austria
[3]Ludwig Boltzmann Institute for Traumatology, The Research Centre in Cooperation with AUVA, Vienna, Austria

*These authors contributed equally to this work.

Corresponding author:
Carina Hromada, Department Life Science Engineering, University of Applied Sciences Technikum Wien, Höchstädtplatz 6, Vienna 1200, Austria.
Email: hromada@technikum-wien.at

stumps, which serve as essential guidance structures for regenerating axons.[4–7]

Despite this intrinsic regenerative potential, functional recovery of severely damaged nerves is rather poor and microsurgical interventions are necessary. The current gold standard for treatment of segmental nerve lesions longer than 5 cm is the use of nerve autografts; however, it is associated with various detrimental side effects.[8,9] In contrast, hollow nerve guidance conduits (NGCs) are the main clinically approved alternative for nerve lesions of up to 4 cm. NGCs provide a controlled microenvironment for nerve regeneration, supporting the accumulation of neurotrophic factors, the formation of an acellular fibrin cable between the nerve stumps and subsequently the proliferation and migration of SCs along the fibrin cable to form aligned SC tracks. These glial bands of Büngner promote axon regeneration from the proximal to the distal nerve stump, followed by remyelination of regenerated axons.[9] However, hollow NGCs fail to promote axon regeneration over longer distances, which is caused by compromised fibrin cable formation, limited infiltration of resident SCs and the inability to maintain the repair phenotype over longer periods.[6,10–12]

Since the adequate formation of bands of Büngner is a major obstacle during regeneration in vivo, numerous attempts have been made to improve the design of NGCs in order to promote endogenous SC migration and alignment. This is accomplished by the addition of topographical guidance structures into the lumen of NGCs, such as longitudinal fibers or filaments, sponges, fillers, or films, as well as longitudinal microgrooves in the inner NGC wall, as reviewed by Daly et al.[9] and Gu et al.[13] However, even these modified NGCs fail to effectively regenerate larger nerve defects, thereby highlighting the importance of creating a more supportive microenvironment for nerve regeneration inside NGCs. Strategies incorporating growth/neurotrophic factors[14–17] or exogenous cells[18–20] have shown great potential in improving functional recovery and nerve regeneration. One promising tissue engineering strategy is to establish nerve grafts that resemble the 3D anisotropic cellular organization. Apart from seeding SCs onto pre-aligned scaffolds,[21–25] other approaches use tethering of cell-laden hydrogels, which induces endogenous cellular tension leading to SC alignment.[26–28] Similarly, Muangsanit et al.[29] introduced the application of gel aspiration-ejection to produce anisotropic Schwann cell-embedded hydrogels. Furthermore, Panzer et al.[30] recently reported the generation of transplantable, tissue-engineered bands of Büngner using collagen-coated microcolumns that induce self-assembly into longitudinally aligned SCs, which supported axon migration in vitro.

Notably, to the best of our knowledge, none of these approaches apply external mechanical stimuli to cell-laden constructs to induce the formation of bands of Büngner.

Considering that peripheral nerves are exposed to mechanical forces during their entire lifespan, such as increasing stiffness and elongation during embryogenesis as well as compressions and stretches during daily activities, mechanical stress likely also plays a pivotal role in regulating SC plasticity.[31–33] Therefore, we hypothesized that the application of strain (i) induces the alignment of SCs along the axis of strain, (ii) leads to the expression of repair-promoting genes, and (iii) that the thereby created bands of Büngner constructs support axon migration. Therefore, the aim of this study was to create tissue-engineered bands of Büngner constructs by subjecting SCs embedded in fibrin hydrogels to mechanical stimulation using the MagneTissue bioreactor, a system which exerts tensile stress onto tissue-engineered constructs by magnetic force transmission.[34,35] Since we observed in previous studies that the application of tensile strain using the MagneTissue bioreactor induces alignment of myotubes along the axis of strain, we hypothesized that mechanical stimulation would likewise induce Schwann cell alignment.[34,35] To assess whether these constructs structurally and functionally mimic the endogenous regenerative capacity of SCs, we analyzed the expression of genes and activation of signaling pathways involved in SC plasticity. Besides analyses of molecular and morphological changes upon mechanical stress, we furthermore aimed to identify the regenerative capacity of the tissue-engineered bands of Büngner constructs by assessing axon migration in an in vitro co-culture model with rat neonatal dorsal root ganglion explants.

Methods

Primary Schwann cell (SC) isolation and cultivation

Primary SCs were isolated from dissected sciatic nerves from male and female Sprague Dawley rats (Janvier Labs, Le Genest-Saint-Isle, France) as previously described.[36] Briefly, after the removal of the epineurium, nerve tissue was enzymatically digested at 37°C and 5% CO_2 overnight in Dulbecco's Modified Eagle's Medium High Glucose (DMEM HG, Lonza, Basel, Switzerland) supplemented with 0.1% collagenase Type I (Sigma Aldrich, St. Louis, MO, USA), 1.25% dispase I (Sigma Aldrich), 3 mM $CaCl_2$, 1% Penicillin/Streptomycin (P/S, Lonza), and 1% Amphotericin B (Lonza). The following day, the dissociated tissue was filtered through a 70 µm cell strainer, DMEM HG with 10% (v/v) fetal calf serum (FCS; GE Healthcare, Chicago, IL, USA) was added and the cell suspension was centrifuged at 300 *g* for 5 min. SCs were seeded in SC medium (SCM) consisting of DMEM HG supplemented with 10% FCS, 1% L-Glutamine (Lonza), 2 µM forskolin (Sigma Aldrich), and 10 ng/ml heregulinβ-1 (PeproTech #100-03, London, UK) onto plates coated with 0.01% poly-L-lysine (Sigma Aldrich).

To remove unwanted fibroblasts, cells were detached with Trypsin-Versene (Lonza) at room temperature for 2 min, centrifuged at 300g for 5 min and incubated on uncoated plates for 30 min at 37°C and 5% CO_2, resulting in the preferential adherence of mostly fibroblasts.[37] The SC-containing supernatant was transferred onto poly-L-lysine-coated plates. Medium was renewed every 2–3 days and SCs were passaged at a confluency of approximately 90%.

Fabrication of Schwann cell-embedded fibrin scaffolds

SCs were embedded in ring-shaped fibrin hydrogels using the clinically approved Tissucol Duo 500 5.0 ml Fibrin Sealant (Baxter, Deerfield, IL, USA) as previously described.[34] Briefly, fibrinogen was diluted to a concentration of 30 mg/ml with SCM. Thrombin was first diluted to 10 U/ml with 40 mM $CaCl_2$, and then further diluted to 4 U/ml with SC suspension. To cast ring-shaped hydrogels, 250 μl of diluted fibrinogen were mixed with 250 μl thrombin/cell suspension, injected into polyoxymethylene scaffold molds (Figure 1(a)), and polymerized at 37°C and 5% CO_2 for 1 h. The ring-shaped scaffolds had a final concentration of 4×10^6 SCs in 15 mg/ml fibrin and 2 U/ml thrombin.

Mechanical stimulation of Schwann cell scaffolds using the MagneTissue bioreactor

The custom-made MagneTissue bioreactor applies uniaxial tensile strain to ring-shaped scaffolds, as previously described.[34,35] For mechanical stimulation, scaffolds were mounted onto custom-made tube inlets with an integrated magnet (Figure 1(b)) and cultured in Falcon 14 ml round bottom polystyrene tubes (BD Biosciences, Bedford, USA) containing 9 ml SCM supplemented with the fibrinolysis inhibitor aprotinin (Baxter) at 100 KIU/ml. Stretching of the scaffolds was achieved by magnetic force transmission between the magnet of the tube inlet and an external magnet in the lower plate of the MagneTissue bioreactor (Figure 1(b)), which can be moved vertically by a stepper motor, thereby resulting in stretching of the scaffolds. After an initial resting period of 48 h, one of the following strain regimes was applied (Figure 1(c)): (i) cyclic strain, that is initial 10% static strain for 48 h, followed by alternating cycles of 0%–12% strain at 250 mHz for 6 h and 0%–3% strain at 250 mHz for 6 h for the remaining 72 h (Figure 1(d)); (ii) static strain, that is application of 10% strain for 48 h, followed by 12% strain for the remaining 72 h; or (iii) ramp strain, that is the application of incremental strain starting at 10%, which was increased by 2% every 24 h, resulting in a final 20% strain at the end of the mechanical stimulation period on day 7. Scaffolds cultivated floating in medium served as unstimulated controls.

RNA isolation from fibrin scaffolds

Samples for RNA isolation were harvested from unstimulated controls and strained constructs 15 min after the onset of mechanical stimulation (d2) as well as 15 min after the last increment of strain on day 7. Fibrin scaffolds were washed in PBS, transferred to 2 ml reinforced Precellys® tubes containing 1.4 mm zirconium oxide beads (Bertin Technologies, Frankfurt, Germany), and subsequently snap-frozen in liquid nitrogen. Samples were homogenized in 1 ml innuSOLV RNA Reagent (IST Innuscreen GmbH, Berlin, Germany) using a Precellys® 24 tissue homogenizer (Bertin Technologies) in three cycles of 5500 rpm for 20 s each. To facilitate lysis, samples were snap-frozen between homogenization cycles and allowed to thaw at room temperature. Following homogenization, samples were centrifuged at 16,000g to pellet fibrin residues. To isolate RNA, homogenized samples were transferred to 2 ml Phasemaker Gel Heavy tubes (Quantabio, Beverly, MA, USA), 200 μl chloroform was added, samples were shaken vigorously for 15 s and incubated at room temperature for 15 min. After centrifugation at 12,000g for 15 min, RNA could be retrieved from the upper aqueous phase, which was separated from the lower organic and interphase by the gel. An equal volume of chloroform was added to the aqueous phase, samples were again incubated for 10 min at room temperature and centrifuged at 12,000g for 15 min. The upper aqueous phase was collected again and RNA was precipitated by adding 600 μl isopropanol and 1.5 μl GlycoBlue™ co-precipitant (Invitrogen, Waltham, MA) for 30 min at room temperature. After centrifugation at 16,000g for 30 min, the supernatant was removed, and RNA pellets were washed three times by adding 1 ml cold 70% ethanol and centrifuging at 12,000g for 10 min each. Subsequently, pellets were air-dried for 10 min at room temperature and RNA was resuspended in 20 μl DEPC-treated distilled water. All centrifugation steps were performed at 4°C.

cDNA synthesis and qPCR

To remove genomic DNA, samples were DNase-treated according to manufacturer's instructions (Thermo Scientific, Waltham, MA, USA). Briefly, 1 μg RNA was incubated with 1 U DNase I and reaction buffer (containing $MgCl_2$) at 37°C for 30 min. Subsequently, DNase was inactivated by incubation at 65°C for 10 min in the presence of EDTA, and the DNase-digested RNA was directly used as a template for reverse transcription using the OneScript® Plus cDNA Synthesis Kit (ABM, Richmond, Canada) with oligo(dT) primers.

qPCR was performed on a qTOWER^{3}G cycler (IST Innuscreen) using the PerfeCTa® Green FastMix® Low ROX (Quantabio). Samples were analyzed in triplicates with 10 ng input cDNA per reaction and 300 nM forward and reverse primers. Data was normalized to the
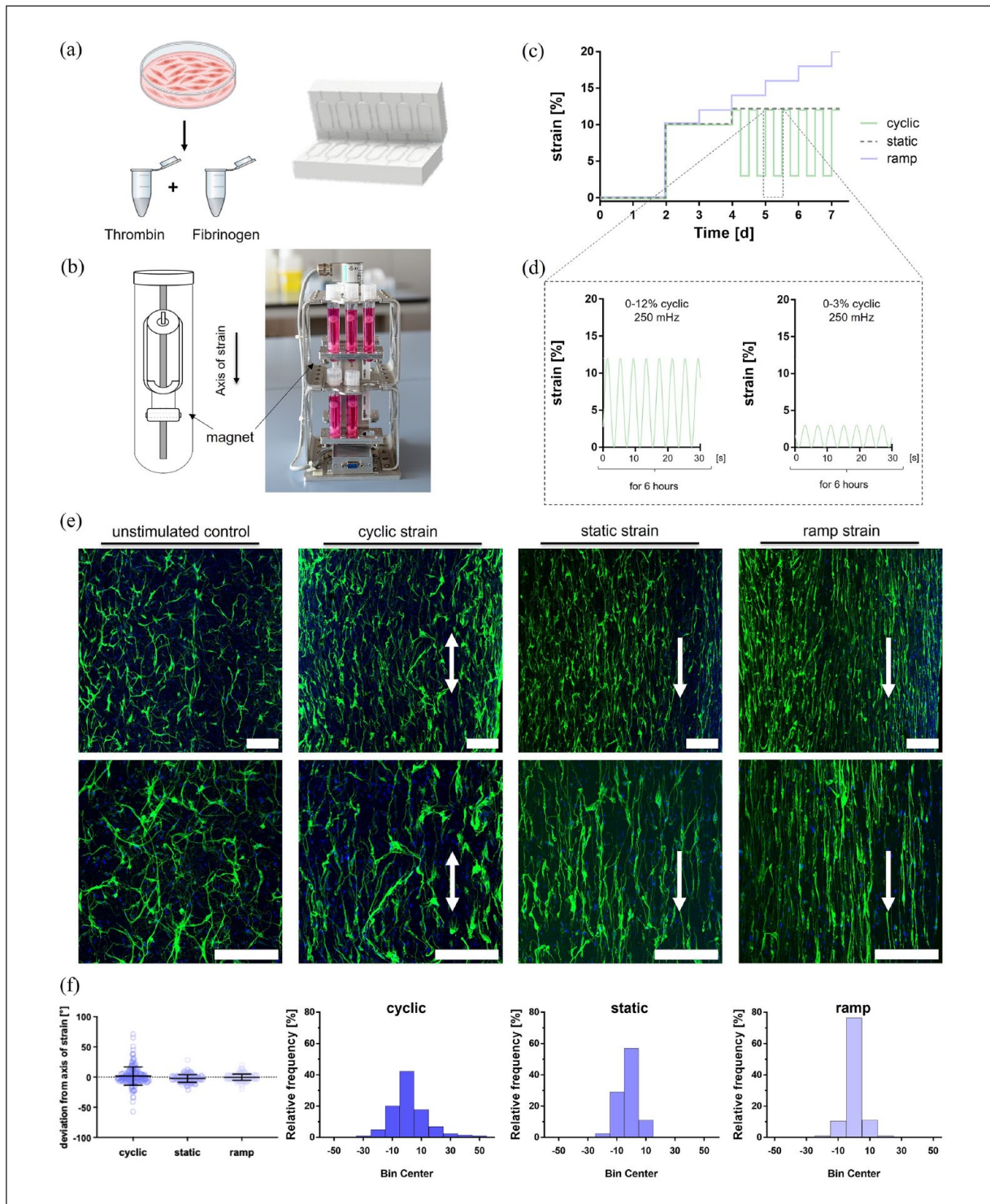
Figure 1. Establishment of tissue-engineered bands of Büngner using the MagneTissue bioreactor: (a) Schwann cells were embedded in ring-shaped fibrin hydrogels using polyoxymethylene molds, (b) Fibrin scaffolds were mounted onto custom-made tube inlets and placed into the MagneTissue bioreactor. Scaffolds were mechanically stimulated via magnetic force transmission between the magnet of the tube inlet and a magnet in the bioreactor's bottom plate (indicated by arrows), which can be moved vertically by a stepper motor, (c) overview of the mechanical stimulation protocols: scaffolds were subjected to a static (gray dashed line, 12% constant static strain), ramp (blue, 2% increments of static strain every 24 h), or cyclic (green, alternating phases of 12% and 3% cyclic strain at 250 mHz for 6 h each, close up in d) simulation protocol, (e) application of different strain protocols strongly influences Schwann cell alignment. In contrast, Schwann cells in unstimulated control scaffolds showed random orientation inside the fibrin hydrogel. Cells were stained for the glial marker S100 (green) and nuclei were counterstained with DAPI (blue). Arrows indicate the axis of strain. Scale bars indicate 200 μm, and (f) analysis of Schwann cell orientation comparing the different strain protocols. The deviation of Schwann cells from the axis of strain (shown as scatter plot with mean ± SD) as well as histograms of relative frequency distributions of Schwann cell orientation is shown. $N = 2$, $n = 2$.

Table 1. Primer sequences used for qPCR analysis.

Target gene	Forward (5′–3′)	Reverse (5′–3′)
BDNF	TCTACGAGACCAAGTGTAATCCCA	CTTATGAACCGCCAGCCAAT
NGF	CTGGGCGAGGTGAACATTAACA	CAGCCTGTTTGTCGTCTGTTGTC
p75^NTR	AAGATGGAGCAATAGACAGGA	CTGAATGCGAAGAGATCCCT
Krox20	CCTACAATCCGCACCACCTG	GAACCTCCTGTCGCAACCCT
MPZ	GTGGTTTACACGGACAGGGAAGT	GGTTGACCCTTGGCATAGTGG
GAPDH	CCGTATCGGACGCCTGGTTA	CCGTGGGTAGAGTCATACTGGAAC

housekeeping gene *GAPDH* and fold changes calculated using the comparative Ct ($\Delta\Delta$Ct) method. Primer sequences[38,39] are listed in Table 1.

Protein isolation and Western blot analysis

Samples for protein isolation were harvested from unstimulated controls and strained constructs 15 min after the onset of mechanical stimulation (d2) as well as 15 min after the last increment of strain on day 7. To isolate protein, fibrin scaffolds were washed with PBS, snap-frozen in liquid nitrogen and homogenized in 1.5 ml tubes using Dstroy® pestles (Biozym, Oldendorf, Germany). Samples were lyzed and further homogenized with 100 µl nonidet P-40 protein isolation buffer (40 mM HEPES (pH 7.9), 120 mM NaCl, 1 mM EDTA (pH 8.0), 10 mM 2-glycerolphosphate, 50 mM NaF, 0.5 mM Na_3VO_4, 1% nonidet P-40 substitute (Sigma Aldrich)) supplemented with protease inhibitors (1 mM phenylmethylsulfonyl fluoride, 2 µg/ml aprotinin, 2 µg/ml leupeptin, 0.3 µg/ml benzamidine chloride, 10 µg/ml trypsin inhibitor) using motorized pellet pestles (DKW Life Sciences, Wertheim, Germany). Total protein was extracted by repeated freeze and thaw cycles in liquid nitrogen, followed by incubation on ice for 1 h and centrifugation at 17,000*g* for 20 min to pellet insoluble material.

For Western blot analysis, equal volumes of denatured protein were resolved on an SDS-polyacrylamide gel (10%) and transferred onto a nitrocellulose membrane (GE Healthcare, Little Chalfont, UK). After blocking for 1 h at room temperature with 5% non-fat milk in Tris-buffered saline containing 0.1% Triton X-100 (Sigma; TBS-T), membranes were incubated in primary antibody solutions in TBS-T containing 5% bovine serum albumin (BSA) at 4°C overnight. Secondary antibody incubation was performed for 1 h at room temperature in 5% non-fat milk in TBS-T. Membranes were scanned with the Odyssey® Fc Imaging System (LI-COR, Lincoln, NE, USA) and signals quantified with Image Studio Lite (LI-COR).

The following primary antibodies were used (all from Cell Signaling Technology, Danvers, MA, USA): Phospho-FAK (Tyr397), 1:1000, #3283; Phospho-p44/42 MAPK (Erk1/2; Thr202/Tyr204), 1:2000, #4370; Phospho-p38 MAPK (Thr180/Tyr182), 1:1000, #4511; and GAPDH, 1:1000, #2118. IRDye® 800CW donkey anti-rabbit was used as secondary antibody at 1:15,000 dilution (LI-COR).

Primary dorsal root ganglion (DRG) isolation

DRG explants were isolated from male and female postnatal day 1 Sprague Dawley rats (Janvier Labs, Le Genest-Saint-Isle, France). The spinal column was excised and dissected to remove the spinal cord. Lumbar level 1–6 (L1–L6) DRG pairs were isolated from intervertebral foramina and stored on ice in PBS supplemented with 1% P/S and 1% Amphotericin B until further processing, but not longer than 2 h.

Co-cultivation of bands of Büngner constructs and dorsal root ganglion explants

Devices for co-cultivation of the tissue-engineered bands of Büngner with DRG explants were composed of a polydimethylsiloxane (PDMS) layer containing six channels with the dimension of the channels of ibidi® sticky-slides VI 0.4 (ibidi GmbH, Gräfelfing, Germany), and plasma-bonded onto glass slides. Tissue-engineered bands of Büngner, generated with the ramp strain protocol, as well as unstimulated control constructs were each cut into two pieces, transferred to separate channels of the co-culture device, and one DRG explant was inserted into each fibrin hydrogel construct. Devices were closed with ibidi® sticky-slides and channels were filled with co-culture medium. Co-culture medium consisted of Neurobasal A medium (Gibco, Thermo Scientific) supplemented with 50 ng/ml recombinant murine β-NGF (Peprotech #450-34), 10 ng/ml heregulinβ−1, 1× B27 (Invitrogen), 1% P/S, 1% Amphotericin B, 1% L-glutamine, and 100 U/ml aprotinin. Medium was exchanged every 2 days. On day 7 of co-cultivation, constructs were fixed for immunofluorescence staining.

Immunofluorescence stainings

Fibrin constructs were fixed in ROTI Histofix (Roth, Karlsruhe, Germany) overnight at 4°C and subsequently

washed three times with distilled water for 5 min each. Hydrogels were permeabilized for 15 min each at room temperature in TBS-T and then PBS-T, and blocked for 1 h at room temperature in PBS-T supplemented with 3% goat serum and 1% BSA. Primary antibody incubations (rabbit polyclonal S100, 1:400, DAKO (Z0311), Santa Clara, CA, US, and mouse monoclonal Neurofilament, 1:100, DAKO (Clone 2F11)) were performed at 4°C overnight in blocking buffer. After washing in PBS-T, secondary antibody stainings (AlexaFluor™ 488 goat anti-mouse IgG (H+L), AlexaFluor™ 488 goat anti-rabbit IgG (H+L), or AlexaFluor™ 594 goat anti-rabbit IgG (H+L), all from Invitrogen) were performed for 1 h at 37°C at a 1:400 dilution in blocking buffer. Nuclei were counterstained with 4′,6-diamidino-2-phenylindole (DAPI) diluted 1:1000 in PBS-T for 10 min at room temperature. Whole constructs were mounted onto glass slides using Fluoroshield (Sigma Aldrich) for fluorescence microscopy.

Microscopical data analysis

Whole-mount constructs were observed with a Leica THUNDER Imager Live Cell & 3D Assay microscope, or an LSM 700 confocal microscope (Zeiss, Oberkochen, Germany). Tile scans of the whole construct area were acquired for tissue-engineered bands of Büngner constructs co-cultured with DRGs.

For analysis of SC alignment after mechanical stimulation, three representative regions of interest (ROI) per sample were imaged. SC alignment was analyzed with the imaging analysis software FIJI[40] using the "Measure" function of the *OrientationJ* plug-in.[41,42] Relative frequencies of orientations were calculated and plotted using GraphPad Prism 7, with 0° being defined as the axis of strain.

Quantification of axon outgrowth in the tile scans was performed using FIJI area measurements ($n = 9$ unstimulated control and $n = 10$ strain). After thresholding for signal in the green channel (neurofilament), the total area of axons was measured. ROIs were defined as area from mid DRG as well as in areas of 1-mm steps beginning at the DRG. The five longest axons (and their respective mean lengths) from each construct were traced and measured with the SNT Neuroanatomy plugin using the pathfinder tool.[43] Only the longest axonal sprouts were measured in case of branching of individual axons.

Statistical analysis

Statistical analyses were performed with GraphPad Prism 7, and data is presented as box and whiskers plots. Data were checked for normal distribution using the Shapiro-Wilk normality test and evaluated using Two-Way ANOVA with Tukey or Sidak post-tests to perform multiple comparisons, or using unpaired *t*-test as indicated in the figure legends.

Results

Application of different strain regimes strongly affects Schwann cell (SC) alignment

For the generation of biomimetic bands of Büngner-like constructs, SCs were embedded in ring-shaped fibrin hydrogels and subjected to different types of tensile strain after an initial resting period of 48 h (Figure 1(a)–(d)). Scaffolds that were cultivated floating inside medium without mechanical strain (unstimulated control) showed a random orientation of SCs inside the hydrogel (Figure 1(e)). To compare the effects of a cyclic and a static stimulation protocol, scaffolds of both groups were first subjected to 10% static strain on day 2 until day 4, and subsequently either subjected to alternating cycles of 12% or 3% cyclic strain for 6 h each at 250 mHz (Figure 1(c) and (d)), or to 12% constant static strain for the remaining 72 h (Figure 1(c)). While the application of cyclic tensile strain only resulted in minor alignment of SCs, static strain induced a higher degree of alignment along the axis of strain (Figure 1(e)). To assess whether SC alignment can be further optimized, we employed a ramp strain protocol with a 2% increase of static strain every day, resulting in 20% relative deformation of scaffolds on day 7 of cultivation (Figure 1(c)). Indeed, this stimulation protocol resulted not only in superior SC alignment, but also in higher SC elongation compared to the other groups (Figure 1(e)). Analysis of SC orientation confirmed these morphological observations: after cyclic stimulation, SC deviation from the axis of strain was $1.7 \pm 15.05°$, $-2.25 \pm 6.35°$ after static and $-0.2 \pm 5.16°$ after ramp strain (Figure 1(f)). Based on these findings, we selected the ramp strain protocol for the generation of highly aligned SC constructs resembling bands of Büngner for all further experiments.

Incremental static strain induces the generation of tissue-engineered bands of Büngner

To more closely investigate the effect of the incremental static mechanical stimulation ("ramp") on SC morphology and orientation, immunofluorescence staining was performed at different time points. Analysis of constructs on the day of preparation of fibrin hydrogels (d0) showed that SCs were evenly distributed and displayed a rounded morphology (Figure 2(a)). Although SCs started to elongate within 24 h after embedding, some cells still remained in their rounded shape (Figure 2(b)), thereby highlighting the importance of the initial 48-h resting period prior to the onset of mechanical stimulation to allow the cells to adapt to their new 3D environment. Two days after encapsulation
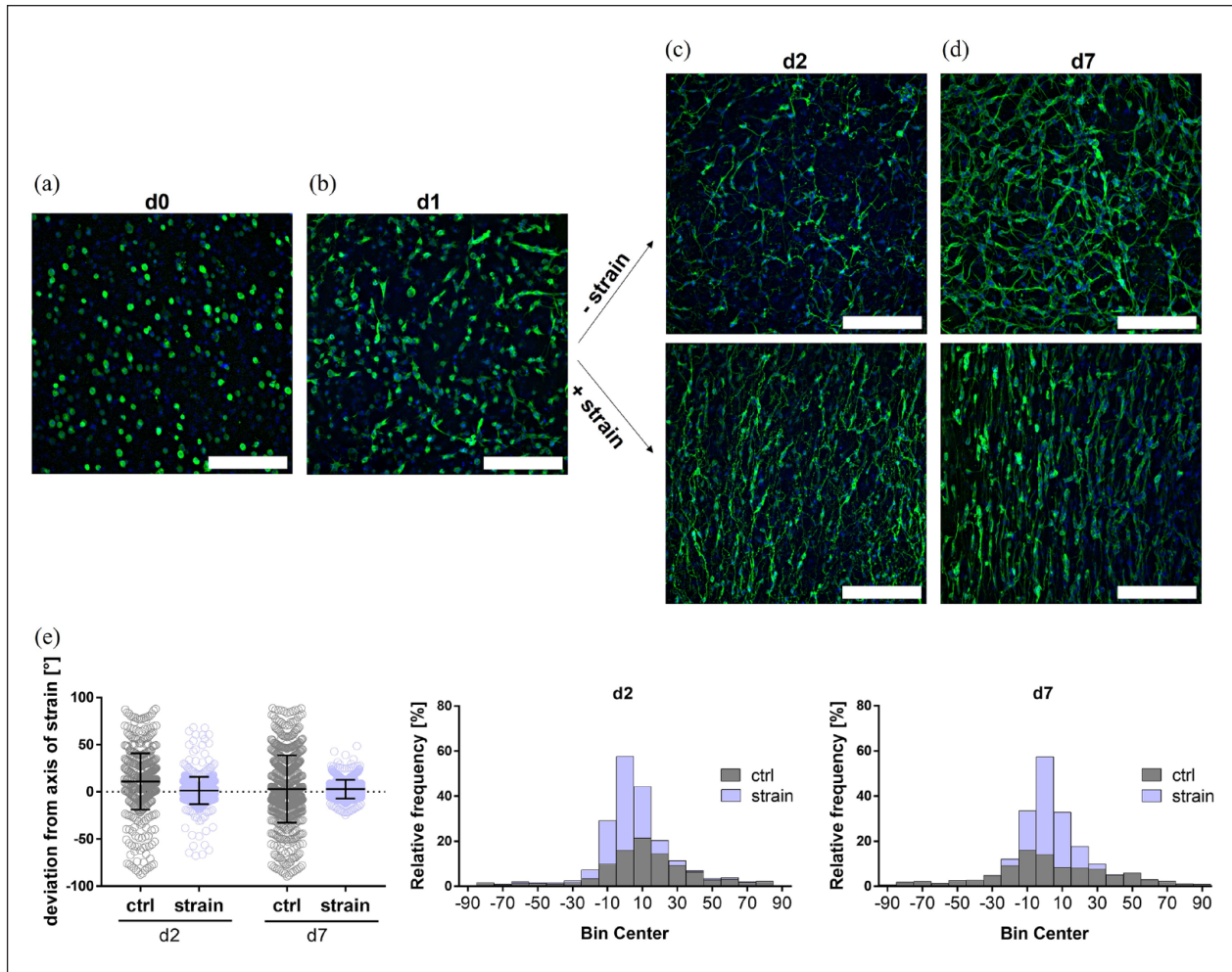
Figure 2. Generation of bands of Büngner-like constructs using mechanical stimulation: (a) directly after embedding in fibrin hydrogels (d0), Schwann cells appeared rounded, (b) after 24 h (d1), most Schwann cells showed an elongated morphology, while some cells still appeared rounded, (c) 2 days after scaffold fabrication, cells showed their characteristic bipolar morphology. Cells in unstimulated control constructs oriented randomly inside the hydrogel, while Schwann cell alignment could already be observed 15 min after the onset of 10% static strain, (d) after 7 days in fibrin hydrogels, Schwann cells remained in their random orientation in unstimulated control constructs, while pronounced alignment of Schwann cells, resembling the formation of bands of Büngner, was induced by the incremental application of strain to 20% on day 7. Cells were stained for the glial marker S100 (green) and nuclei were counterstained with DAPI (blue). Scale bars indicate 200 μm, and (e) analysis of Schwann cell orientation in unstimulated controls (gray) and strained constructs (blue) on day 2 and day 7 of cultivation, shown as deviation from the axis of strain (scatter plot with mean ± SD) and as relative frequency distribution histograms. $N = 4$, $n = 4$.

in fibrin, SCs showed their characteristic bi- or multipolar, elongated morphology. As expected, SC constructs that were cultivated as unstimulated controls showed random orientation inside fibrin hydrogels, whereas initial alignment of cells along the axis of strain could be observed as early as 15 min after the (initial) onset of 10% static strain (Figure 2(c)). Static strain was subsequently incremented by 2% every day, resulting in the application of 20% static strain on day 7 of cultivation inside fibrin hydrogels, which induced the formation of highly aligned SCs along the axis of strain that resemble bands of Büngner-like structures. In contrast, unstimulated SCs displayed a random orientation

even after 7 days inside the fibrin hydrogels (Figure 2(d)). Quantitative analysis of SC orientation further corroborated these morphological observations, showing that SCs in unstimulated control constructs covered a broad range of orientations on both day 2 and day 7 of cultivation (deviation from axis of strain $11.1 \pm 29.77°$ and $3.09 \pm 35.6°$, respectively). In contrast, mechanically stimulated constructs showed that already 15 min of static tensile stress induced SC alignment, resulting in an orientation deviating $1.48 \pm 14.44°$ from the axis of strain. As expected, alignment was further improved throughout the cultivation period with incremental strain, resulting in $3.02 \pm 9.95°$
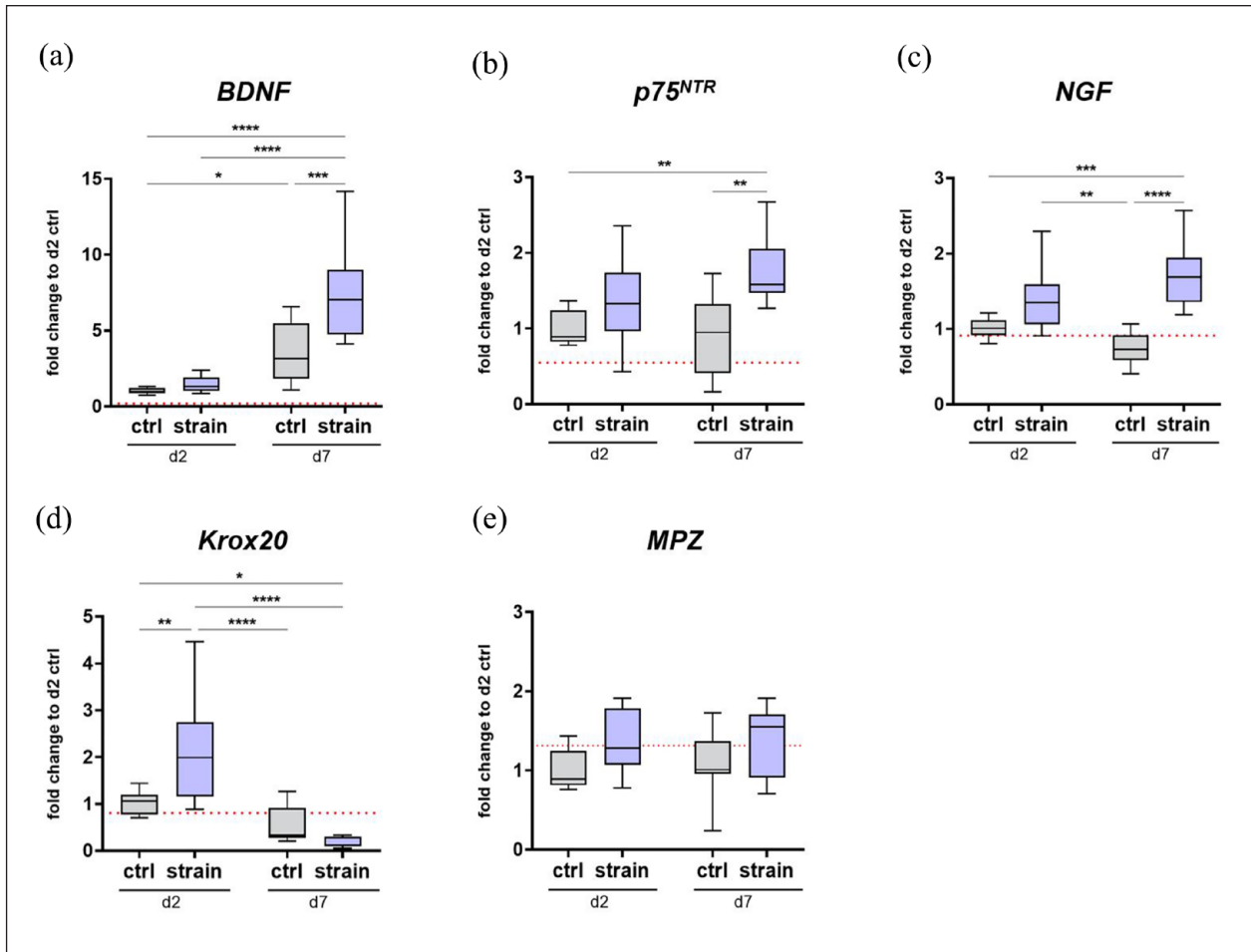
Figure 3. Mechanical stimulation enhances the expression of pro-regenerative markers. mRNA expression levels of the pro-regenerative genes *BDNF* (a), *p75*[NTR] (b), and *NGF* (c), as well as of the myelin-associated *Krox20* (d) and *MPZ* (e) were assessed 15 min after the onset of strain (d2) and 15 min after the last increment to 20% strain (d7) by qPCR. *GAPDH* was used as a housekeeping gene. Dotted red lines indicate expression fold change of Schwann cells grown in 2D relative to d2 control. Data shown as Box and Whisker plot (min to max). $N = 3$, $n = 9$; Two-way ANOVA with Tukey's multiple comparison test. *$p < 0.05$. **$p < 0.01$. ***$p < 0.001$. ****$p < 0.0001$.

deviation of SC orientation from the axis of strain on day 7 (Figure 2(e)).

Mechanical stimulation of Schwann cells enhances the expression of pro-regenerative genes

Following the morphological observation of pronounced SC alignment after the application of incremental static strain, we aimed to assess whether the occurrence of these tissue-engineered bands of Büngner is accompanied by a repair SC phenotype on a transcriptional level. Therefore, we analyzed the expression of different pro-regenerative as well as myelin-associated markers that are known to be involved in the process of adaptive cellular reprograming. Expression of the pro-regenerative genes *BDNF, p75*[NTR], and *NGF* was significantly increased at the end of the mechanical stimulation period (d7 strain) compared to

unstimulated controls of both day 2 and day 7 (Figure 3(a)–(c)). These findings indicate that mechanical stimulation of SCs not only induces cellular alignment resembling the naturally occurring bands of Büngner, but also promotes the expression of genes associated with the repair SC phenotype.

Furthermore, the increase of pro-regenerative markers was accompanied by a significant, fivefold expression downregulation of *Krox20*, the key transcription factor for SC myelination, at the end of the mechanical stimulation period compared to day 2 controls. Interestingly, *Krox20* expression was significantly upregulated 15 min after the onset of 10% static strain (d2 strain); however, this upregulation was only transient and followed by a significant downregulation of *Krox20* expression in day 7 constructs (Figure 3(d)). In contrast, the expression of *MPZ* did not show significant changes throughout the cultivation period (Figure 3(e)), indicating the general pro-regenerative
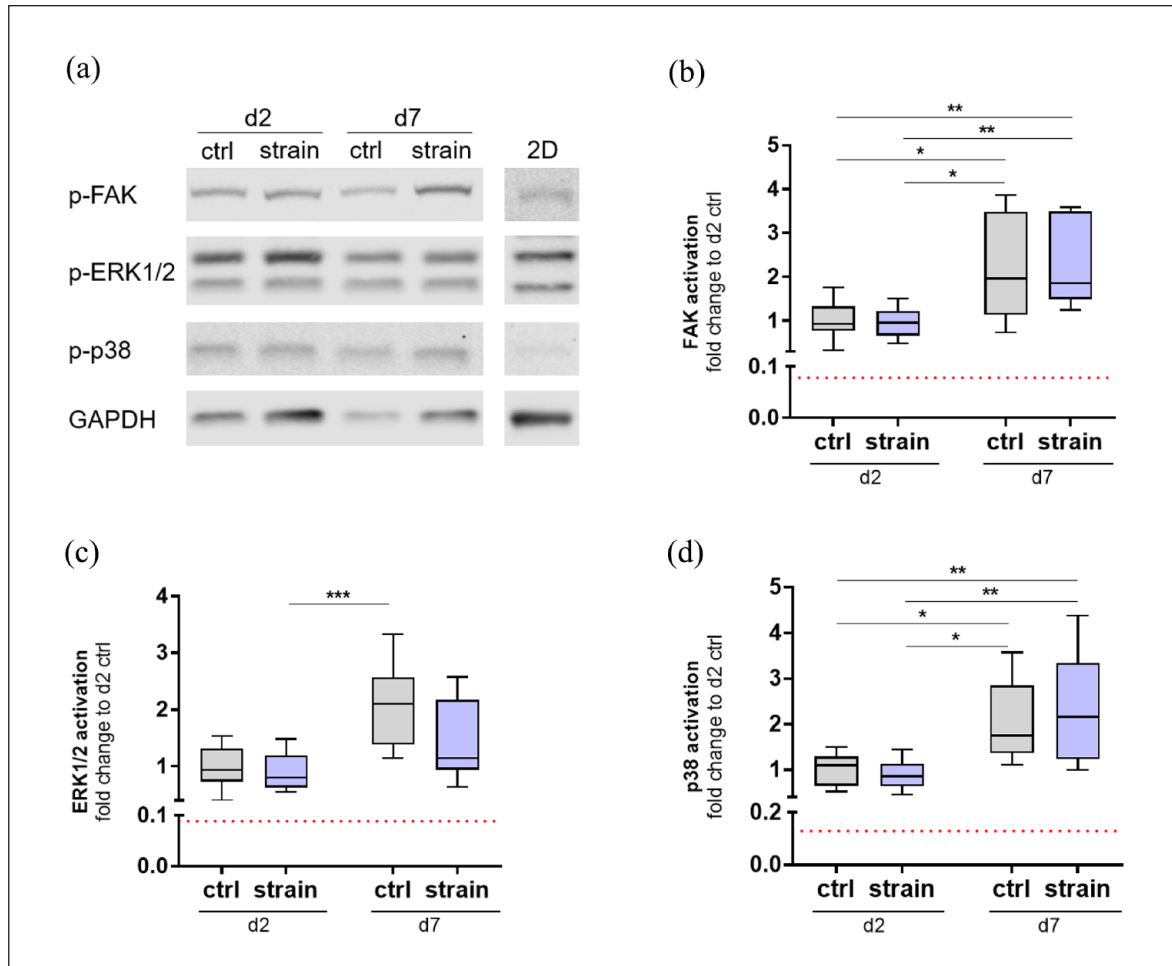
Figure 4. Activation of signaling pathways involved in the stress response and Schwann cell plasticity: (a) representative Western blot scans (of three independent experiments) are shown. Samples were lysed 15 min after the onset of strain (d2) and 15 min after the last increment to 20% strain (d7). Activation of FAK (b), ERK1/2 (c), and p38 (d) was calculated as the ratio of phosphorylated protein to the loading control GAPDH and normalized to d2 control. Dotted red lines indicate protein expression fold change of Schwann cells grown in 2D relative to d2 control. Data shown as box and whisker plot (min to max). $N = 3$, $n = 9$; Two-way ANOVA with Tukey's multiple comparison test.
$*p < 0.05$. $**p < 0.01$. $***p < 0.001$.

nature of SCs in vitro in the absence of axons. Moreover, expression of *BDNF* and *p75*[NTR] was increased in both control and strained scaffolds compared to cells cultivated in 2D without fibrin (Figure 3(a) and (b), dotted red line), whereas expression of *Krox20* and *MPZ* seemed to be unaffected by cell cultivation in fibrin (Figure 3(c) and (d), dotted red line).

3D cultivation in fibrin but not strain activates mechanosensing pathways

The ability of cells to sense mechanical cues and the subsequent conversion into biochemical signals strongly impacts cell behavior, including morphology, adhesion, migration, regeneration, and disease. While current research mainly focuses on the influence of substrate stiffness and topography, studies investigating the effect of

tensile stress on SCs are scarce. Therefore, we here aimed to investigate the effects of mechanical stimulation on SCs by analyzing signaling pathways known to be involved in stress response as well as in the regulation of SC plasticity (Figure 4(a)). Phosphorylation of focal adhesion kinase (FAK), which is involved in mechano-sensing and cell migration, was significantly increased in d7 constructs compared to d2 controls (Figure 4(b)), and furthermore, this increase was stronger in strained than control constructs ($p = 0.012$ ctrl vs $p = 0.0077$ strain). In addition, since mitogen-activated protein kinase (MAPK) signaling pathways have been proposed to be involved in both SC plasticity and response to extracellular stimuli, we aimed to assess the activation of the MAPK signal transducers extracellular signal-regulated kinases 1 and 2 (ERK1/2) and p38. Although we observed higher ERK1/2 activation in all 3D fibrin constructs compared to 2D

cultured SCs, the application of mechanical strain did not affect the activation of this pathway (Figure 4(c)). While p38 activation was also significantly increased in both control and strained constructs on d7 compared to d2 controls (Figure 4(d)), this increase was stronger in strained than control constructs ($p = 0.0388$ ctrl vs $p = 0.0054$ strain). Furthermore, activation of all signaling pathways was higher in fibrin constructs compared to cells cultivated in 2D without fibrin (Figure 4(b)–(d), dotted red line), thereby indicating that the 3D fibrin environment affects mechanosensing pathways.

Tissue-engineered bands of Büngner guide sensory axon migration of dorsal root ganglion explants

Since we showed that mechanical stimulation leads to an enhanced pro-regenerative SC phenotype as well as pronounced alignment of cells on a molecular and morphological level, we subsequently aimed to evaluate the effect of these tissue-engineered bands of Büngner on sensory neurite outgrowth and guidance. Therefore, the ring-shaped SC constructs were retrieved from the MagneTissue bioreactor and cut into two pieces. To study axon regeneration, we inserted DRGs from neonatal rats into one end of the construct and cultivated them for additional 7 days without mechanical stimulation in self-made PDMS devices. As expected, longitudinally aligned SCs seemed to guide migrating axons, thereby promoting superior axon outgrowth and elongation (Figure 5). In contrast, axon outgrowth in unstrained controls appeared more disorganized, most likely as a result of randomly oriented SCs (Figure 5). Furthermore, alignment of SCs could be maintained even 7 days after the end of the application of strain, and this stability of cellular anisotropy represents an important prerequisite for clinical application.

Quantification of axon outgrowth revealed that the total area covered by axons was significantly higher in strained constructs compared to unstrained controls (Figure 6(a)). Moreover, the tissue-engineered bands of Büngner constructs resulted in longer sensory axon migration (Figure 6(b)). Furthermore, constructs with mechanically aligned SCs facilitated axon migration over longer distances (Figure 6(c)).

These findings demonstrate that mechanical stimulation induces longitudinal alignment of SCs, which was stable even after withdrawal from mechanical stimulation, resembling putative bands of Büngner-like structures. Moreover, longitudinal alignment by mechanical stimulation also leads to enhanced expression of repair-promoting genes and furthermore promotes sensory axon outgrowth. These findings indicate that the generation of tissue-engineered bands of Büngner-like structures using mechanical stimulation might offer great therapeutic potential for implantation into patients, and could furthermore serve as
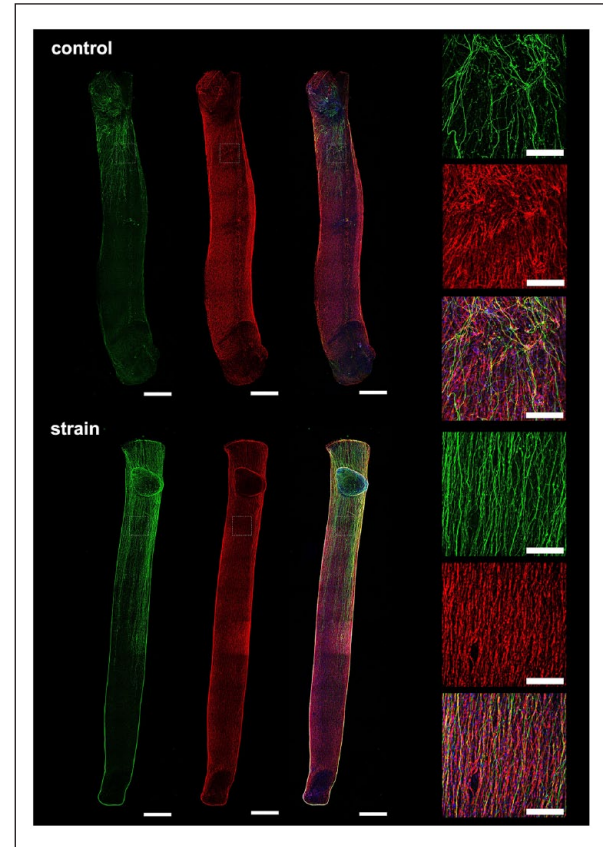

Figure 5. Axon outgrowth from rat neonatal dorsal root ganglion explants inserted into 3D tissue-engineered bands of Büngner constructs and unstimulated control hydrogels after 7 days of co-cultivation. Unorganized axon outgrowth was observed in unstimulated control constructs (top panel), while highly aligned axon migration was present in mechanically aligned Schwann cell constructs (bottom panel). Constructs were stained for Neurofilament (green) to visualize axons and the glial marker S100 (red) to visualize Schwann cells; nuclei were counterstained with DAPI (blue). Scale bars indicate 1 mm or 100 μm for whole mount scans or magnified areas, respectively.

a promising and physiologically relevant in vitro peripheral nerve model.

Discussion

Peripheral nerve injuries can have a devastating impact on patients' quality of life, and treatment of nerve lesions remains a major challenge, often resulting in slow and even incomplete recovery. In addition, the use of autologous nerve transplants—still the current gold standard treatment—is associated with detrimental side effects, such as donor side morbidity, neuroma formation, or limited donor nerve availability.[9] Hence, tissue engineering strategies aim to develop suitable alternatives, such as decellularized allografts and NGCs. However, these acellular options typically fail to achieve functional recovery
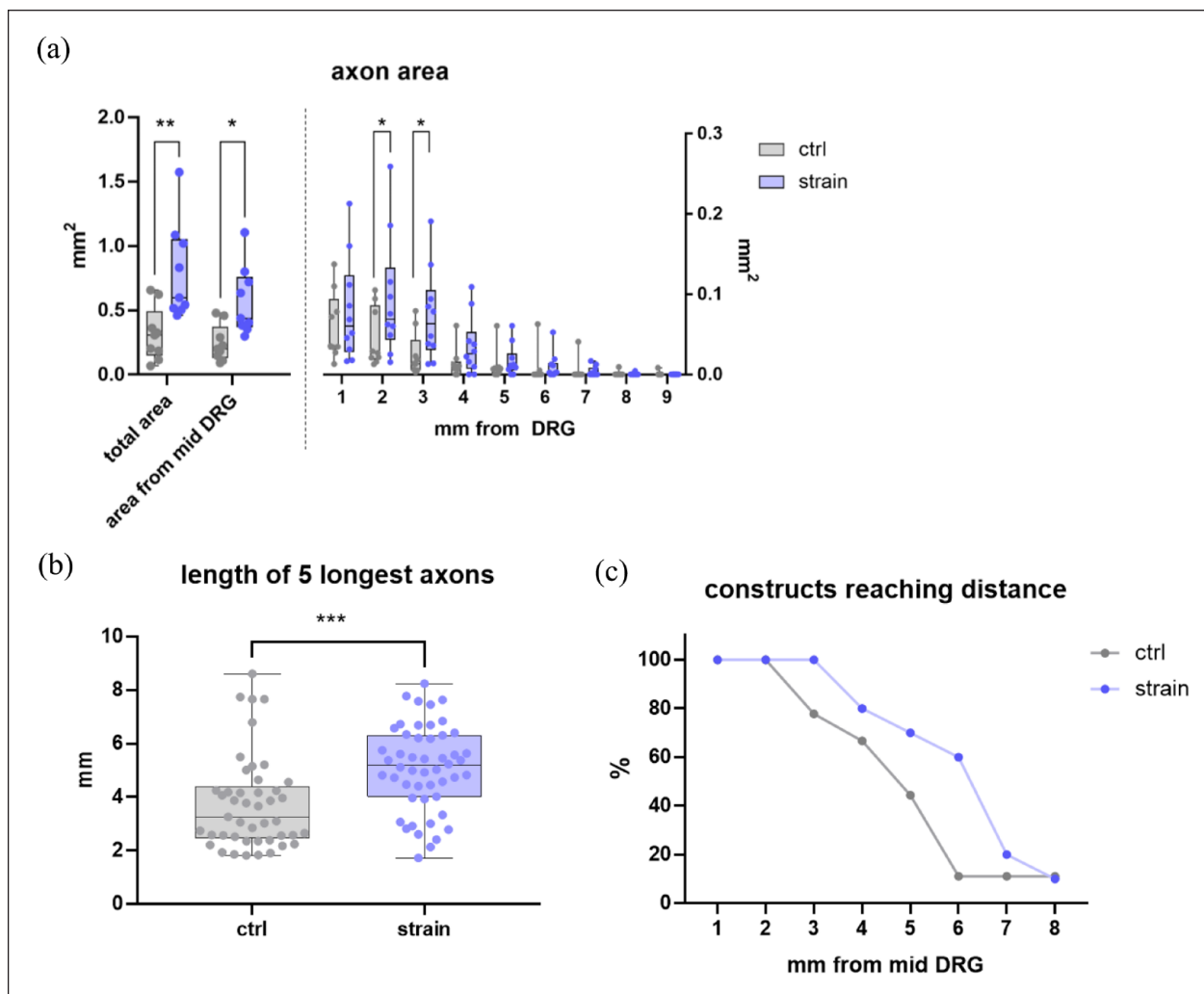
Figure 6. Quantification of axon outgrowth 7 days after inserting rat neonatal dorsal root ganglion explants into tissue-engineered bands of Büngner and control constructs: (a) the area covered by axons was quantified for whole constructs as well as in 1-mm segments from the dorsal root ganglion, (b) quantification of the five longest axons observed in each construct, (c) percentage of constructs reaching the specified distance. Data shown as Box and Whiskers (min to max with all data points) (a and b) or as connected line (c). $N = 3$, $n = 9$, or $n = 10$ for control and strain, respectively. Two-way ANOVA with Sidak's multiple comparison test (a) and unpaired *t*-test (b).
*$p < 0.05$. **$p < 0.01$. ***$p < 0.001$. ****$p < 0.0001$.

of segmental nerve lesions exceeding 3 cm, presumably due to limited SC infiltration into the graft, often associated with loss of repair phenotype and senescence.[11,44] Therefore, the addition of exogenous SCs expressing and maintaining a repair phenotype presents a promising strategy to enhance peripheral nerve repair. In this study, we aimed to establish tissue-engineered bands of Büngner constructs via the application of mechanical strain to fibrin-based hydrogels containing primary SCs. The thereby created tissue-engineered bands of Büngner could be used as luminal fillers of NGCs in order to potentially replace nerve autografts, currently used in clinics. To the best of our knowledge, we for the first time show that direct mechanical stimulation of SCs not only induces

longitudinal alignment of cells along the axis of strain resembling bands of Büngner, but also leads to the expression of a pronounced repair SC phenotype. Both the expression of regeneration-promoting factors and provision of physical guidance structures supported axon migration over several millimeters in vitro.

These 3D tissue-engineered bands of Büngner were created using a custom-made strain bioreactor system, called MagneTissue, initially developed by our group to engineer skeletal muscle-like constructs.[34,35] With this bioreactor, controlled mechanical strain (% of deformation, frequency, cycle numbers) can be applied to cells embedded in hydrogels via magnetic force transmission. Here, we used primary SCs isolated from rat sciatic nerves

embedded in fibrin hydrogels. Fibrin is particularly suitable for peripheral nerve tissue engineering, since the formation of a fibrin cable between the lesioned nerve stumps during the initial stages of nerve repair provides an important provisional matrix for SC proliferation and migration, leading to the formation of bands of Büngner that bridge the defect.[45,46] In fact, early in vivo studies suggested that SC proliferation and migration was inhibited due to the lack of fibrin cable formation in larger defects, thereby hindering nerve regeneration.[47,48]

Although several approaches attempted to create aligned SC constructs to mimic bands of Büngner structures, mainly based on seeding of cells on structured surfaces,[21–25] we, to the best of our knowledge, for the first time report the successful establishment of 3D tissue-engineered bands of Büngner-like tissue structures by incorporating active mechanical stimulation in a 3D SC culture model. We showed that the type of tensile stress applied strongly influenced SC alignment, as static strain induced more pronounced alignment than cyclic strain. In particular, the application of an incremental static strain ("ramp") protocol was found to be superior in inducing SC alignment resembling bands of Büngner compared to constant static strain. Since fibrin is a viscoelastic biomaterial, the hydrogel likely adapted to the applied load upon constant strain, thereby causing the effect of the mechanical stimulus to diminish over time in the static strain group, a phenomenon that was mitigated by a daily increase in the load of 2%.

Considering that peripheral nerves are exposed to mechanical forces during their entire lifespan—ranging from increasing stiffness during morphogenesis to stretches and compressions from daily activities—mechanical stress likely also plays a pivotal role in regulating SC plasticity.[31–33] Nevertheless, studies on SC mechanobiology are still scarce and mostly focus on how stiffness and topography affect SC adhesion, shape, migration, or myelination,[49–51] but only rarely on how they are affected by tensile stress. Similar to our results, Zhang et al.[38] reported that subjecting a 2D SC monolayer to cyclic tensile stress in vitro induced downregulation of the myelin transcription factor *Krox20*, as well as an upregulation of BDNF expression and secretion. Chen et al.[52] embedded SCs in 3D auxetic gelatin-methacryloyl hydrogels and subjected them to cyclic tensile stress, which resulted in increased proliferation, increased GDNF and NGF protein expression, as well as increased NGF secretion. However, none of these studies investigated the effect of strain on cell alignment, nor on axon regeneration.

Here, we provide evidence that static strain induces the expression of a repair SC phenotype, which was characterized by the upregulation of the pro-regenerative genes *BDNF, p75^{NTR}*, and *NGF* along with a downregulation of the pro-myelinating transcription factor *Krox20* compared to unstimulated controls. Among the pro-regenerative

genes investigated, *BDNF* showed the strongest upregulation in response to mechanical stimulation. The neurotrophins BDNF and NGF belong to the neurotrophic factor family and bind to the tropomyosin receptor kinase (Trk) receptors with high affinity, which is known to promote axon survival and growth during nerve regeneration. In addition, neurotrophins also interact with the p75^{NTR} receptor with low affinity, which is not expressed in intact nerves, but rapidly upregulated upon injury.[53–55] In fact, p75^{NTR} has been reported to play a dual, controversial role during peripheral nerve regeneration, with some studies finding that p75^{NTR} is essential for nerve regeneration,[56–58] while others showed its effect on impaired regeneration.[59–61] As summarized in reviews, p75^{NTR} signaling is highly complex and the responses it elicits seem to largely depend on its interaction partner: while complexing with the Trk receptors increases neurotrophin affinity and consequently enhances axon survival and growth, independent p75^{NTR} signaling has been associated with apoptosis and impaired nerve regeneration.[54,55,62] In our study, we hypothesize that the increased *p75^{NTR}* expression—together with enhanced *BDNF* and *NGF* expression—in mechanically strained constructs contributed to improved regeneration, since we observed improved axon elongation in these constructs and could not see signs of enhanced apoptosis.

Although we here, for the first time, describe the generation of highly aligned SC constructs using active external mechanical stimulation, a more thorough characterization of the established structures is required to corroborate that the formed structures indeed represent the formation of bands of Büngner. Hence, we aim to analyze N-Cadherin expression at intercellular SC junctions[63,64] in future experiments. Moreover, we also aim to investigate whether the expression of repair-promoting genes induced by mechanical stimulation of SCs can be maintained after the withdrawal of strain.

Furthermore, we also aimed to assess signaling pathways involved in stress response and SC reprograming. Interestingly, the investigated signaling pathways did not seem to be greatly affected by the application of strain. However, cultivation of SCs in 3D fibrin hydrogels seemed to induce activation of FAK and the MAPK-ERK1/2 and p38 pathways, all of which are involved in SC plasticity.[65–69] It has been suggested that ERK1/2 activation initiates the SC response to nerve lesions by inducing SC proliferation, dedifferentiation, and myelin breakdown.[66,67] Furthermore, Akassoglou et al.[70] reported that cellular binding to fibrin induces ERK1/2 phosphorylation in SCs, which is in accordance with our observation of increased ERK1/2 activation in SC fibrin constructs compared to cells cultivated in 2D in the absence of fibrin. Similarly, we also observed increased p38 activation in control as well as strained samples on day 7 compared to day 2 control constructs; however, p38 phosphorylation was stronger

in strained constructs compared to unstimulated controls, suggesting that mechanical stimulation might support the SC repair phenotype via the p38 MAPK pathway. Indeed, p38 has been shown to mediate SC plasticity by promoting SC dedifferentiation, demyelination as well as alignment.[68,69] Furthermore, we also aimed to analyze FAK phosphorylation, since its activation by integrins triggers important mechanosensing signaling pathways that regulate cell adhesion, migration, and survival.[71,72] In this study, we observed significantly increased FAK phosphorylation in SC constructs irrespective of the application of strain. This might have been triggered by binding of the SCs' integrin receptor $\alpha_V\beta_8$ to the fibrin RGD sequence.[73] Moreover, FAK was shown to sustain the SCs' proliferative state and to prevent premature differentiation.[74] Taken together, our findings suggest that our established constructs show repair-promoting characteristics, as evidenced by the expression of pro-regenerative genes as well as by the upregulation of signaling pathways known to be involved in SC reprograming.

Based on our findings that the application of strain induces repair-promoting characteristics on a molecular level, that is the expression of pro-regenerative genes and activation of signaling pathways known to mediate SC reprograming, as well as morphologically, that is the formation of bands of Büngner, we further assessed axonal outgrowth from neonatal rat DRG explants to prove the pro-regenerative potential of the tissue-engineered bands of Büngner. DRGs inserted into aligned SC constructs showed extensive and significantly longer axon outgrowth compared to control constructs. As discussed by Panzer et al.,[30] the previously reported axon growth rate on aligned SCs in vitro was limited to 334 μm/day.[25,75,76] In another study, Malheiro et al.[77] reported an axonal growth rate of <430 μm/day on constructs with SCs seeded onto electrospun scaffolds, which were embedded into fibrin hydrogels. Here, we observed an average maximal growth rate of 727 μm/day when analyzing the constructs after 7 days of culture using DRGs embedded in a rather dense 3D fibrin matrix. In contrast, Panzer et al.[30] could observe axon migration of even 1.166 μm/day after 4 days, but on the intraluminal surface of SC-seeded hollow hydrogel-based micro-columns. However, we must emphasize that we determined the axon growth rate based on the axon length on day 7 of culture and hence, we cannot exclude the possibility that axon growth is faster during the first days of culture than in later time points.

Furthermore, aligned SCs seemed to improve axon directionality compared to randomly oriented SCs in control constructs. Remarkably, immunofluorescence staining revealed that SC alignment could be maintained even after 7 days of withdrawal from mechanical strain, which is an important prerequisite for application in vivo. This highlights the great therapeutic potential of our tissue-engineered bands of Büngner constructs, which might provide a promising alternative to nerve autografts when used as

an intraluminal filler in NGCs. One major advantage compared to the limited availability of nerve autografts is the variable length of tissue-engineered bands of Büngner constructs we are able to engineer with our approach (currently 3 cm in length), while the required thickness can be adjusted by stacking several constructs together. In future studies, we aim to compare the regenerative potential of the tissue-engineered bands of Büngner with nerve autografts in a rat peripheral nerve defect model. In addition to the therapeutic potential, our tissue-engineered bands of Büngner hold great promise for the establishment of a biomimetic in vitro peripheral nerve model. In fact, there is a growing demand for physiologically relevant 3D nerve tissue models to improve clinical translatability of novel drugs and reduce animal experimentation. Additionally, such models offer helpful platforms to study pathologic and regenerative processes of the peripheral nervous system. Consequently, to establish such a model we will strive to induce myelination in the co-cultures of tissue-engineered bands of Büngner with DRGs. At this point, we cannot predict the SCs' remyelination ability in our constructs, since myelination in rodent models has been described to occur only after approximately 28 days in vitro with the addition of ascorbic acid,[78] whereas our co-culture model was only kept in culture for 7 days.

In conclusion, in this study, we could show for the first time that mechanical stimulation can be used to induce the formation of tissue-engineered bands of Büngner-like structures in a hydrogel matrix, and cellular anisotropy was stable even after the end of the mechanical stimulation protocol. Moreover, mechanical stimulation also promoted the expression of a pronounced and sustained repair SC phenotype, which promoted axon migration. These constructs therefore not only hold great therapeutic potential for implantation into patients but could also serve as a promising and physiologically relevant in vitro peripheral nerve tissue model for drug screening or to investigate diseases as well as regenerative processes.

Author contributions

C.H.: data acquisition, analysis, and interpretation; manuscript draft and revision. D.S.-H.: data acquisition and interpretation; manuscript revision. J.T., M.Q.N., and M.P.: data interpretation; manuscript revision. D.H. and A.T.-W.: study design; data analysis and interpretation; manuscript revision.

Declaration of conflicting interests

The author(s) declared the following potential conflicts of interest with respect to the research, authorship, and/or publication of this article: CH and ATW disclose a potential conflict of interest

related to the research presented in this study. They have submitted a patent application for a technology that is related to a component used in the research described in this paper.

Informed consent, ethical approval, and human rights

This study did not involve human or animal studies.

ORCID iD

Carina Hromada https://orcid.org/0000-0001-6583-1372
Janine Tomasch https://orcid.org/0000-0002-1689-7145

Data availability statement

Original data underlying this study will be provided upon request.

References

1. Aman M, Zimmermann KS, Thielen M, et al. An epidemiological and etiological analysis of 5026 peripheral nerve lesions from a European level I trauma center. *J Pers Med* 2022; 12: 1673.
2. Huckhagel T, Nüchtern J, Regelsberger J, et al. Nerve injury in severe trauma with upper extremity involvement: evaluation of 49,382 patients from the TraumaRegister DGU® between 2002 and 2015. *Scand J Trauma Resusc Emerg Med* 2018; 26: 76.
3. Bergmeister KD, Große-Hartlage L, Daeschler SC, et al. Acute and long-term costs of 268 peripheral nerve injuries in the upper extremity. *PLoS ONE* 2020; 15: e0229530.
4. Jessen KR and Mirsky R. The repair Schwann cell and its function in regenerating nerves: Repair Schwann cell and its function in regenerating nerves. *J Physiol* 2016; 594: 3521–3531.
5. Jessen KR and Arthur-Farraj P. Repair Schwann cell update: adaptive reprograming, EMT, and stemness in regenerating nerves. *Glia* 2019; 67: 421–437.
6. Jessen KR and Mirsky R. The success and failure of the schwann cell response to nerve injury. *Front Cell Neurosci* 2019; 13: 33.
7. Gomez-Sanchez JA, Pilch KS, Van Der Lans M, et al. After nerve injury, lineage tracing shows that myelin and remak schwann cells elongate extensively and branch to form repair schwann cells, which shorten radically on remyelination. *J Neurosci* 2017; 37: 9086–9099.
8. Siemionow M and Brzezicki G. Chapter 8 current techniques and concepts in peripheral nerve repair. *Int Rev Neurobiol* 2009; 87: 141–172.
9. Daly W, Yao L, Zeugolis D, et al. A biomaterials approach to peripheral nerve regeneration: bridging the peripheral nerve gap and enhancing functional recovery. *J R Soc Interface* 2012; 9: 202–221.
10. Sulaiman OAR and Gordon T. Role of chronic schwann cell denervation in poor functional recovery after nerve injuries and experimental strategies to combat it. *Neurosurgery* 2009; 65: A105–A114.
11. Saheb-Al-Zamani M, Yan Y, Farber SJ, et al. Limited regeneration in long acellular nerve allografts is associated with increased Schwann cell senescence. *Exp Neurol* 2013; 247: 165–177.
12. Painter MW, Brosius Lutz A, Cheng Y-C, et al. Diminished Schwann cell repair responses underlie age-associated impaired axonal regeneration. *Neuron* 2014; 83: 331–343.
13. Gu X, Ding F, Yang Y, et al. Construction of tissue engineered nerve grafts and their application in peripheral nerve regeneration. *Prog Neurobiol* 2011; 93: 204–230.
14. Lackington WA, Kočí Z, Alekseeva T, et al. Controlling the dose-dependent, synergistic and temporal effects of NGF and GDNF by encapsulation in PLGA microparticles for use in nerve guidance conduits for the repair of large peripheral nerve defects. *J Control Rel* 2019; 304: 51–64.
15. Madduri S, Di Summa P, Papaloïzos M, et al. Effect of controlled co-delivery of synergistic neurotrophic factors on early nerve regeneration in rats. *Biomaterials* 2010; 31: 8402–8409.
16. Wood MD, MacEwan MR, French AR, et al. Fibrin matrices with affinity-based delivery systems and neurotrophic factors promote functional nerve regeneration. *Biotech Bioeng* 2010; 106: 970–979.
17. Wood MD, Gordon T, Kim H, et al. Fibrin gels containing GDNF microspheres increase axonal regeneration after delayed peripheral nerve repair. *Regen Med* 2013; 8: 27–37.
18. Burks SS, Diaz A, Haggerty AE, et al. Schwann cell delivery via a novel 3D collagen matrix conduit improves outcomes in critical length nerve gap repairs. *J Neurosurg* 2021; 135: 1241–1251.
19. McGrath AM, Novikova LN, Novikov LN, et al. BD™ PuraMatrix™ peptide hydrogel seeded with Schwann cells for peripheral nerve regeneration. *Brain Res Bull* 2010; 83: 207–213.
20. Gonzalez-Perez F, Hernández J, Heimann C, et al. Schwann cells and mesenchymal stem cells in laminin- or fibronectin-aligned matrices and regeneration across a critical size defect of 15 mm in the rat sciatic nerve. *J Neurosurg Spine* 2018; 28: 109–118.
21. Das S, Sharma M, Saharia D, et al. Electrospun silk-polyaniline conduits for functional nerve regeneration in rat sciatic nerve injury model. *Biomed Mater* 2017; 12: 045025.
22. Bozkurt A, Brook GA, Moellers S, et al. In vitro assessment of axonal growth using dorsal root ganglia explants in a novel three-dimensional collagen matrix. *Tissue Eng* 2007; 13: 2971–2979.
23. Bozkurt A, Deumens R, Beckmann C, et al. In vitro cell alignment obtained with a Schwann cell enriched microstructured nerve guide with longitudinal guidance channels. *Biomaterials* 2009; 30: 169–179.

24. Lietz M, Dreesmann L, Hoss M, et al. Neuro tissue engineering of glial nerve guides and the impact of different cell types. *Biomaterials* 2006; 27: 1425–1436.

25. Daud MFB, Pawar KC, Claeyssens F, et al. An aligned 3D neuronal-glial co-culture model for peripheral nerve studies. *Biomaterials* 2012; 33: 5901–5913.

26. Phillips JB, Bunting SCJ, Hall SM, et al. Neural Tissue Engineering: A Self-Organizing Collagen Guidance Conduit. *Tissue Eng* 2005; 11: 1611–1617.

27. Georgiou M, Bunting SCJ, Davies HA, et al. Engineered neural tissue for peripheral nerve repair. *Biomaterials* 2013; 34: 7335–7343.

28. Schuh CMAP, Day AGE, Redl H, et al. An optimized collagen-fibrin blend engineered neural tissue promotes peripheral nerve repair. *Tissue Eng Part A* 2018; 24: 1332–1340.

29. Muangsanit P, Day A, Dimiou S, et al. Rapidly formed stable and aligned dense collagen gels seeded with Schwann cells support peripheral nerve regeneration. *J Neural Eng* 2020; 17: 046036.

30. Panzer KV, Burrell JC, Helm KVT, et al. Tissue engineered bands of büngner for accelerated motor and sensory axonal outgrowth. *Front Bioeng Biotechnol* 2020; 8: 580654.

31. Belin S, Zuloaga KL and Poitelon Y. Influence of mechanical stimuli on schwann cell biology. *Front Cell Neurosci* 2017; 11: 347.

32. Rosso G, Young P and Shahin V. Implications of schwann cells biomechanics and mechanosensitivity for peripheral nervous system physiology and pathophysiology. *Front Mol Neurosci* 2017; 10: 345.

33. Fornaro M, Marcus D, Rattin J, et al. Dynamic environmental physical cues activate mechanosensitive responses in the repair schwann cell phenotype. *Cells* 2021; 10: 425.

34. Heher P, Maleiner B, Prüller J, et al. A novel bioreactor for the generation of highly aligned 3D skeletal muscle-like constructs through orientation of fibrin via application of static strain. *Acta Biomater* 2015; 24: 251–265.

35. Tomasch J, Maleiner B, Hromada C, et al. Cyclic tensile stress induces skeletal muscle hypertrophy and myonuclear accretion in a 3D model. *Tissue Eng Part A* 2023; 29: 257–268.

36. Hromada C, Hartmann J, Oesterreicher J, et al. Occurrence of lymphangiogenesis in peripheral nerve autografts contrasts schwann cell-induced apoptosis of lymphatic endothelial cells in vitro. *Biomolecules* 2022; 12: 820.

37. Weiss T, Taschner-Mandl S, Ambros PF, et al. Detailed protocols for the isolation, culture, enrichment and immunostaining of primary human schwann cells. In: Monje PV, Kim HA (eds) *Schwann eells*. New York, NY: Springer, pp.67–86.

38. Zhang L, Yang X, Yue Y, et al. Cyclic mechanical stress modulates neurotrophic and myelinating gene expression of Schwann cells. *Cell Prolif* 2015; 48: 59–66.

39. Hercher D, Kerbl M, Schuh CMAP, et al. Spatiotemporal differences in gene expression between motor and sensory autografts and their effect on femoral nerve regeneration in the rat. *Front Cell Neurosci* 2019; 13: 182.

40. Schindelin J, Arganda-Carreras I, Frise E, et al. Fiji: an open-source platform for biological-image analysis. *Nat Methods* 2012; 9: 676–682.

41. Fonck E, Feigl GG, Fasel J, et al. Effect of aging on elastin functionality in human cerebral arteries. *Stroke* 2009; 40: 2552–2556.

42. Gesellchen F, Bernassau AL, Déjardin T, et al. Cell patterning with a heptagon acoustic tweezer – application in neurite guidance. *Lab Chip* 2014; 14: 2266–2275.

43. Arshadi C, Günther U, Eddison M, et al. SNT: a unifying toolbox for quantification of neuronal anatomy. *Nat Methods* 2021; 18: 374–377.

44. Poppler LH, Ee X, Schellhardt L, et al. Axonal growth arrests after an increased accumulation of schwann cells expressing senescence markers and stromal cells in acellular nerve allografts. *Tissue Eng Part A* 2016; 22: 949–961.

45. Williams LR, Longo FM, Powell HC, et al. Spatial-temporal progress of peripheral nerve regeneration within a silicone chamber: parameters for a bioassay. *J Comp Neurol* 1983; 218: 460–470.

46. Carvalho CR, Oliveira JM and Reis RL. Modern trends for peripheral nerve repair and regeneration: beyond the hollow nerve guidance conduit. *Front Bioeng Biotechnol* 2019; 7: 337.

47. Williams LR, Danielsen N, Müller H, et al. Exogenous matrix precursors promote functional nerve regeneration across a 15-mm gap within a silicone chamber in the rat. *J Comp Neurol* 1987; 264: 284–290.

48. Williams LR and Varon S. Modification of fibrin matrix formation in situ enhances nerve regeneration in silicone chambers. *J Comp Neurol* 1985; 231: 209–220.

49. Gu Y, Ji Y, Zhao Y, et al. The influence of substrate stiffness on the behavior and functions of Schwann cells in culture. *Biomaterials* 2012; 33: 6672–6681.

50. Urbanski MM, Kingsbury L, Moussouros D, et al. Myelinating glia differentiation is regulated by extracellular matrix elasticity. *Sci Rep* 2016; 6: 33751.

51. Poitelon Y, Lopez-Anido C, Catignas K, et al. YAP and TAZ control peripheral myelination and the expression of laminin receptors in Schwann cells. *Nat Neurosci* 2016; 19: 879–887.

52. Chen Y-W, Wang K, Ho C-C, et al. Cyclic tensile stimulation enrichment of Schwann cell-laden auxetic hydrogel scaffolds towards peripheral nerve tissue engineering. *Mater Des* 2020; 195: 108982.

53. Frostick SP, Yin Q and Kemp GJ. Schwann cells, neurotrophic factors, and peripheral nerve regeneration. *Microsurgery* 1998; 18: 397–405.

54. Meeker R and Williams K. The p75 neurotrophin receptor: at the crossroad of neural repair and death. *Neural Regen Res* 2015; 10: 721.

55. Bibel M and Barde Y-A. Neurotrophins: key regulators of cell fate and cell shape in the vertebrate nervous system. *Genes Dev* 2000; 14: 2919–2937.

56. Song X-Y, Zhang F-H, Zhou FH, et al. Deletion of p75NTR impairs regeneration of peripheral nerves in mice. *Life Sci* 2009; 84: 61–68.

57. Tomita K, Kubo T, Matsuda K, et al. The neurotrophin receptor p75NTR in Schwann cells is implicated in remyelination and motor recovery after peripheral nerve injury. *Glia* 2007; 55: 1199–1208.

58. Anton ES, Weskamp G, Reichardt LF, et al. Nerve growth factor and its low-affinity receptor promote Schwann cell migration. *Proc Natl Acad Sci USA* 1994; 91: 2795–2799.

59. Boyd JG and Gordon T. The neurotrophin receptors, trkB and p75, differentially regulate motor axonal regeneration. *J Neurobiol* 2001; 49: 314–325.

60. McGregor C, Sabatier M and English A. Early regeneration of axons following peripheral nerve injury is enhanced if p75^{NTR} is eliminated from the surrounding pathway. *Eur J Neurosci* 2021; 53: 663–672.

61. Scott ALM and Ramer MS. Schwann cell p75NTR prevents spontaneous sensory reinnervation of the adult spinal cord. *Brain* 2010; 133: 421–432.

62. Meeker R and Williams K. Dynamic nature of the p75 neurotrophin receptor in response to injury and disease. *J Neuroimmune Pharmacol* 2014; 9: 615–628.

63. Ribeiro-Resende VT, Koenig B, Nichterwitz S, et al. Strategies for inducing the formation of bands of Büngner in peripheral nerve regeneration. *Biomaterials* 2009; 30: 5251–5259.

64. Wanner IB and Wood PM. N-Cadherin mediates axon-aligned process growth and cell–cell interaction in rat schwann cells. *J Neurosci* 2002; 22: 4066–4079.

65. Chang H-M, Shyu M-K, Tseng G-F, et al. Neuregulin facilitates nerve regeneration by speeding schwann cell migration via ErbB2/3-dependent FAK pathway. *PLoS ONE* 2013; 8: e53444.

66. Harrisingh MC, Perez-Nadales E, Parkinson DB, et al. The Ras/Raf/ERK signalling pathway drives Schwann cell dedifferentiation. *EMBO J* 2004; 23: 3061–3071.

67. Napoli I, Noon LA, Ribeiro S, et al. A central role for the ERK-signaling pathway in controlling schwann cell plasticity and peripheral nerve regeneration in vivo. *Neuron* 2012; 73: 729–742.

68. Yang DP, Kim J, Syed N, et al. p38 MAPK activation promotes denervated schwann cell phenotype and functions as a negative regulator of schwann cell differentiation and myelination. *J Neurosci* 2012; 32: 7158–7168.

69. Fragoso G, Robertson J, Athlan E, et al. Inhibition of p38 mitogen-activated protein kinase interferes with cell shape changes and gene expression associated with Schwann cell myelination. *Exp Neurol* 2003; 183: 34–46.

70. Akassoglou K, Yu W-M, Akpinar P, et al. Fibrin inhibits peripheral nerve remyelination by regulating schwann cell differentiation. *Neuron* 2002; 33: 861–875.

71. Guan J-L. Role of focal adhesion kinase in integrin signaling. *Int J Biochem Cell Biol* 1997; 29: 1085–1096.

72. Bauer MS, Baumann F, Daday C, et al. Structural and mechanistic insights into mechanoactivation of focal adhesion kinase. *Proc Natl Acad Sci USA* 2019; 116: 6766–6774.

73. A Chernousov M and J Carey D. αVβ8 integrin is a Schwann cell receptor for fibrin. *Exp Cell Res* 2003; 291: 514–524.

74. Grove M and Brophy PJ. FAK is required for schwann cell spreading on immature basal lamina to coordinate the radial sorting of peripheral axons with myelination. *J Neurosci* 2014; 34: 13422–13434.

75. Armstrong SJ, Wiberg M, Terenghi G, et al. ECM molecules mediate both schwann cell proliferation and activation to enhance neurite outgrowth. *Tissue Eng* 2007; 13: 2863–2870.

76. Sun M, McGowan M, Kingham PJ, et al. Novel thin-walled nerve conduit with microgrooved surface patterns for enhanced peripheral nerve repair. *J Mater Sci Mater Med* 2010; 21: 2765–2774.

77. Malheiro A, Morgan F, Baker M, et al. A three-dimensional biomimetic peripheral nerve model for drug testing and disease modelling. *Biomaterials* 2020; 257: 120230.

78. Callizot N, Combes M, Steinschneider R, et al. A new long term in vitro model of myelination. *Exp Cell Res* 2011; 317: 2374–2383.